CHAPTER 2

THEORETICAL BACKGROUND

2.1 Theories of liquid crystalline phases :

The theories of liquid crystalline phases have been described in details in several books [1-5]. I am giving below, in a nutshell, the salient features of the mean-field theories of nematic and smectic A phases as developed by Maier-Saupe [6] and McMillan [7,8] respectively.

2.1.1 Maier-Saupe theory for nematic phase:

It has been mentioned in the previous chapter that the rod like molecules of a liquid crystalline substance tend to align their long axes along a preferred direction, called the director $\overleftrightarrow{n}$, in a mesophase. The distribution of the molecular long axes about the director is given by an orientational distribution function $f(\cos\theta)$, assuming cylindrical symmetry of the mesophase, where θ is the angle between the director and the molecular long axis. If the molecules have no head to tail asymmetry, then $\overleftrightarrow{n} = -\overleftrightarrow{n}$, and $f(\cos\theta)$ is an even function of $\cos\theta$. The distribution function can also be written as [9]:

$$f(\cos\theta) = \sum_{L \text{ even}} (2L+1)/2 \langle P_L(\cos\theta)\rangle P_L(\cos\theta) \qquad 2.1$$

where $P_L(\cos\theta)$ are the L^{th} even order Legendre polynomials, and $\langle P_L(\cos\theta)\rangle$ are the statistical average given by

$$\langle P_L(\cos\theta)\rangle = \int_0^1 P_L(\cos\theta)\, f(\cos\theta)\, d(\cos\theta) \Big/ \int_0^1 f(\cos\theta)\, d(\cos\theta) \qquad 2.2$$

$\langle P_L\rangle$ are called the orientational order parameters, of which the first member, i.e, $\langle P_2\rangle$ is commonly called the order parameter. $\langle P_2\rangle$ is equal to one for perfectly oriented sample and is equal to zero for randomly oriented, i.e, isotropic liquid.

The angular part of the generalised mean-field potential as felt by a rigid rod like molecule can be written as

$$V(\cos\theta) = \sum_{L,\text{even}} u_L \langle P_L \rangle P_L(\cos\theta), \qquad 2.3$$

where U_L are functions of distance between the central molecule and its neighbours only. Maier and Saupe [6] assumed that the potential can be taken to be the leading term only of the series in equation 2.3, ie.,

$$V(\cos\theta) = -v \langle P_2 \rangle P_2(\cos\theta) \qquad 2.4$$

Hence, the orientational distribution function $f(\cos\theta)$ and the partition function Z are given by (k being the Boltzmann constant),

$$f(\cos\theta) = Z^{-1} \exp [-V(\cos\theta)/kT] \qquad 2.5$$

$$Z = \int_0^1 \exp [-V(\cos\theta)/kT] \, d(\cos\theta) \qquad 2.6$$

Substituting the value of $f(\cos\theta)$ as in equation (2.5) to equation (2.2), we get for L = 2,

$$\langle P_2 \rangle = Z^{-1} \int_0^1 P_2(\cos\theta) \exp [\langle P_2 \rangle P_2(\cos\theta)/T^*] \, d(\cos\theta) \qquad 2.7$$

where $T^* = v/kT$

As equation (2.7) contains $\langle P_2 \rangle$ on both the sides, a self consistent solution of it is sought. For all values of T^* (or T) $\langle P_2 \rangle = 0$ is a solution, while for $T^* < .22284$, two other solutions of $\langle P_2 \rangle$ appear. Obviously, the state with minimum free energy is the stable one. It can be shown that for $T^* < .22019$, a state with $\langle P_2 \rangle > 0$ is stable one, which can be identified with nematic phase, whereas for $T^* > .22019$, $\langle P_2 \rangle = 0$, gives the equilibrium state, which is the isotropic liquid.

The nematic-isotropic liquid transition occurs at $T_c^* = 0.22019$ and $\langle P_2 \rangle_c = 0.4289$, according to the Maier Saupe theory. Thus, this transition is always of the first order. Values of $\langle P_2 \rangle$ as a function of T^* can be calculated easily by solving equation (2.7) iteratively. For many liquid crystals the Maier- Saupe $\langle P_2 \rangle$ values

agree quite well with those found experimentally.

2.1.2. McMillan's theory for smectic A phase:

In smectic A phase, there is a periodic density variation along the layer normal (z direction) in addition to the orientational distribution of the molecular axes. Hence, the nomalised distribution function can be written, in this case, as [Ref.1, chapter 7]

$$f(\cos\theta),z) = \sum_{L,\text{even}} \sum_{n} A_{L,n} P_L(\cos\theta) \cos(2\pi n z/d) \qquad 2.8$$

$$\text{with} \int_{-1}^{1} \int_{0}^{d} f(\cos\theta,z)\, dz\, d(\cos\theta) = 1 \qquad 2.9$$

as normalising condition, d being the layer thickness.

McMillan [7,8], following Kobayashi [10,11], assumed a model potential of the following form

$$V_M(\cos\theta,z) = -v[\, \delta\alpha\tau \cos(2\pi z/d) + \{\eta + \alpha\delta \cos(2\pi z/d)\} P_2(\cos\theta)\,] \qquad 2.10$$

where α and δ are two parameters of the potential. $\eta = \langle P_2(\cos\theta)\rangle$, $\tau = \langle \cos(2\pi z/d)\rangle$ and $\sigma = \langle P_2(\cos\theta) \cos(2\pi z/d)\rangle$ are the orientational, translational and mixed order parameters respectively, and $\langle\ \rangle$ denotes statistical average of the quantities inside.

The distribution function can be written as

$$f_M(\cos\theta,z) = Z^{-1} \exp[\, -V_M(\cos\theta,z)/kT\,] \qquad 2.11$$

where the partition function

$$Z = \int_0^1 \int_0^d \exp[\, -V_M(\cos\theta,z)/kT\,]\, d(\cos\theta)\, dz \qquad 2.12$$

Once again, three self consistency equations containing η, τ and σ

can be written and solved iteratively.
Out of several solutions, the equilibrium state is identified by the minimum value of free energy.

In general, we get the following three cases:

Case I $\eta = 0, \tau = 0, \sigma = 0$, isotropic liquid.
Case II $\eta \neq 0, \tau = 0, \sigma = 0$, nematic liquid crystal.
Case III $\eta \neq 0, \tau \neq 0, \sigma \neq 0$, smectic liquid crystal.

while nematic-isotropic transition is always first order, the smectic A - nematic transition can be either first order ($T_{AN}/T_{NI} > 0.88$) or second order ($T_{AN}/T_{NI} < 0.88$), where T_{AN} and T_{NI} are the smectic A- nematic and nematic-isotropic transition temperatures respectively.

2.2 Identification of phases:

2.2.1 Texture studies:

The textures are the patterns which are observed microscopically on liquid crystalline samples , usually in polarised light. For the determination of transition temperatures and the identification of liquid crystalline phases, observation of textures is an important tool for the liquid crystal physicist. Commonly they are observed in thin layers (≈ 10-20 micrometer) between two glass slides. These are nothing but the defects of the phase structure which are generated by the combined action of the phase structure and the surrounding glass plates (surface phenomena). Change in texture at a particular temperature indicates the occurrence of phase transition. For low cooling or heating rates the transition temperatures observed are generally identical. Again for a given structure, different textures can exist, depending on the special conditions in preparations of the sample. Although there exists different textures in liquid crystals, the individual texture of an observed phase often allow a first estimation as to general phase type. In table 2.1 the most frequently observed textures of the various phase types is given

[12].

It is seen that, homeotropic textures are observed only in phases of nematic, smectic A and smectic B (both orthogonal smectic phases). In smectic C, smectic F and smectic I phases (all tilted smectic phases) broken focal conic texture are observed. The in-layer ordered smectic phases show mosaic texture. Classification of different liquid crystalline phases by the observation of textures alone is often ambiguous, and other methods are needed to support it.

Table 2.1 : Textures of the various phase types [13].

	PHASE TYPE											
TEXTURE	E	H	G	B	F	I	C*	C	A	BP[b]	N*	N
Isotropic										x		
Homeotropic				x			x		x		x	x
Homogeneous						x		x	x			x
Marbled												x
Stepped drops	x			x			x		x			
Mosaic	x	x	x	x	x	x				x		
Schlieren					x	x		x				x
Simple focal conic				x[a]					x		x	
Broken focal conic	x[a]		x		x	x		x				

* Chiral phase

a Paramorphic textures

b Blue phase

2.3. X-ray diffraction from mesophases:

X-ray diffraction from mesomorphic phases has been reviewed by many workers [14-19], specially by Vainshtein [14] and Leadbetter [19].

Unoriented nematic phase shows x-ray diffraction pattern which is a uniform halo just like that of an isotropic liquid. This is due to the fact that, generally a liquid crystal sample consists of a large number of domains, the molecules being aligned within each domain in a preferred direction, i.e., the director, but there is no preferred direction for the sample as a whole and naturally, x-ray diffraction pattern has a symmetry of revolution around the direction of x-ray beam.

The principal features of the x-ray pattern of a nematic sample, which is oriented perpendicular to the incident x-ray beam, is shown in the figures 2.1 (a) and (b). The main halo has split into two crescents for each of which the intensity is maximum in the equatorial direction, i.e., perpendicular to the director (optic axis). These crescents are formed mainly due to the nearest neighbour intermolecular scattering and the corresponding Bragg angle is a measure of lateral intermolecular distance. The angular distribution of the x-ray intensity (Figure 2.1(a)), $I(\psi)$ vs. ψ, also gives the orientational distribution function $f(\cos\theta)$ and order parameters $\langle P_L \rangle$.

In the meridional direction, at a much smaller Bragg angle, a pair of crescents arc also seen. They are connected with apparent molecular length. Sometimes, the inner difuse crescents are replaced by rather sharp spots. The presence of the sharp spots indicates smectic like clusters in the nematic phase. These clusters are called "Cybotactic" groups and are formed due to smectic fluctuations in the nematic phase.

The x-ray diffraction pattern from smectic A phase is shown in Figure 2.1(b) and is very similar to cybotactic nematic. The meridional spots are formed due to Bragg reflection from the layers and provide the value of the layer thickness. Since smectic A can have only quasi-long range order (QLRO) along its layer normal [3,20], the second order Bragg reflections in the

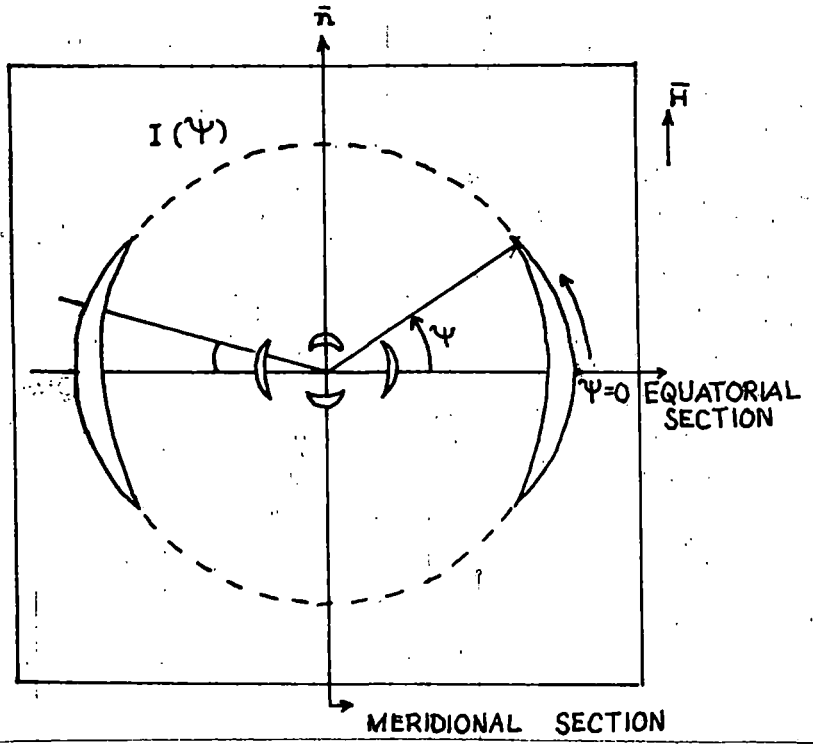

Figure 2.1(a). Schematic representation of the x-ray diffraction pattern of an oriented nematic liquid crystal.

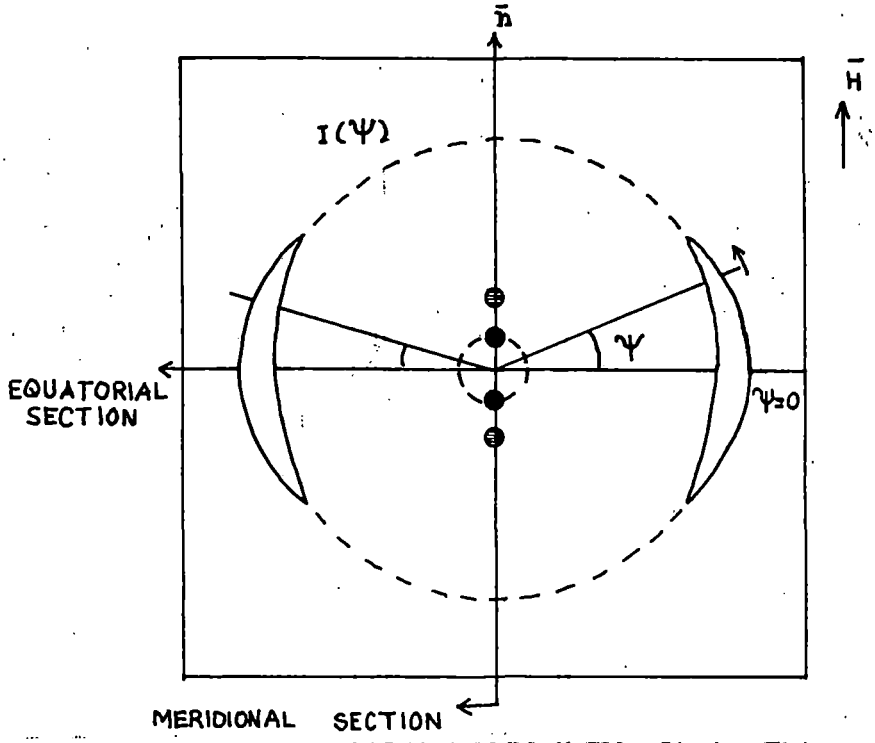

Figure 2.1(b). Schematic representation of the x-ray diffraction pattern of an oriented smectic A liquid crystal.

meridional direction are generally very weak and are often absent in the x-ray photographs. When present, these second order reflections provide a method for calculating τ, the translational order parameter.

We, also, get some faint diffuse rings (crescents) in our x-ray photographs, which may be due to (a) interatomic scattering, (b) next nearest neighbour intermolecular scattering and (c) effect of white radiation contained in Ni filtered Cu radiation. We are generally not concerned with those diffraction patterns.

2.3.1 Experimental technique and data analysis: x-ray diffraction studies.

X-ray diffraction photographs were obtained with the apparatus described below using nickel filtered CuK_α radiation in the transmission geometry on a film [21], using a flat plate camera designed in our laboratory by Jha et al [21] (Figure 2.2). X- ray diffraction photographs were taken at different temperatures in the presence of a magnetic field. The camera has the provisions to change the collimator (2), spacer (15) and sample container (8). The sample was taken in a thin-walled lithium glass capillary of 1 mm diameter. The capillary containing sample was placed in a brass block. The temperature of the block was controlled within $\pm$ 0.5°C by a temperature controller (Indotherm MD 401). The sample was first heated to the isotropic phase and magnetic field was applied parallel to the capillary axis. The substance was allowed to cool to the desired temperature in the presence of the magnetic field. The magnetic field was kept on during the x-ray diffraction experiment. The strength of the magnetic field was measured previously by a gaussmeter (ECIL model GH 867). X- ray beam was collimated by a collimeter of aperture 0.8 mm. A Ni filter of thickness 0.009 mm was used to obtain predominent CuK_α radiation of wavelength 1.542Å. When the temperature reached equlibrium then the x-ray tube was switched on. Photographs were taken at various constant temperatures. In case of the determination of orientational order parameters the sample to film distance was maintained at about 6 cm. To obtain better accuracy in the layer

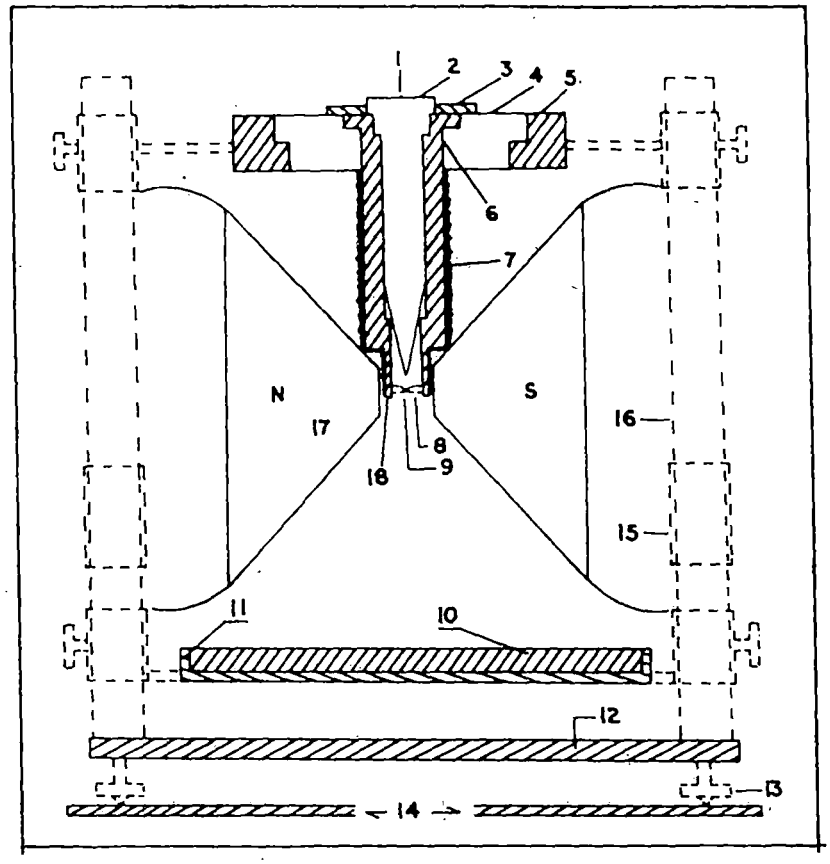

Figure 2.2. Sectional diagram of the x-ray diffraction camera. 1. X-ray, 2. Collimator, 3. Brass ring, 4. Ring of sindanyo board, 5. Brass ring, 6. Cylindrical brass chamber, 7. Asbestos insulation and heater winding, 8. Specimen holder and thermocouple, 9. Sample, 10. Film cassette, 11. Film cassette holder, 12. Base plate, 13. Levelling screw, 14. Brass plates over the coils of the electromagnet, 15. Removable spacer, 16. Supporting brass stand, 17. Pole pieces, 18. Asbestos insulation.

thickness measurement, x-ray diffraction photographs of inner spots were taken with sample to film distance increased to about 9 cm.

For the determination of the exact distance between the sample and film I took aluminium-powder photograph. The Bragg angle corresponding to the (hkl) reflecting plane for Al can be determined by [22]

$$\sin \theta' = (\lambda/2a)(h^2 + k^2 + l^2) \qquad 2.13$$

Thus measuring the diameter of the diffraction rings corresponding to (111) and (200) reflections [11] and values of Bragg angles from 2.13, the actual distance between sample and the film can be found out from the relation

$$\tan 2\theta' = \frac{\text{Radius of the ring}}{\text{Sample to film distance}} \qquad 2.14$$

The correction term was then calculated and used to measure the actual sample to film distance, from the apparent distance due to the spacers.

(a). Conversion of optical density to x-ray intensity :

The optical density of the x- ray photographs was measured by a microdensitometer (Carl Zeiss MD 100) which has a potentiometric recording (K200) facility for linear scanning. X-ray intensity values are then obtained from the conversion of the corresponding optical density values by a method given by Klug and Alexander [23]. Multiple film technique was used, where an intensity scale was prepared by exposing different portion of a film to x-ray coming through a rectangular opening with exposure times 2, 5, 10, 20, etc. secs. Optical density values for different exposure times were then measured with the microdensitometer. After subtracting the optical density of the unexposed film a graph of optical density versus exposure time, i.e, x-ray intensity (which is proportional to the time of exposure) was drawn as shown in figure 2.3.

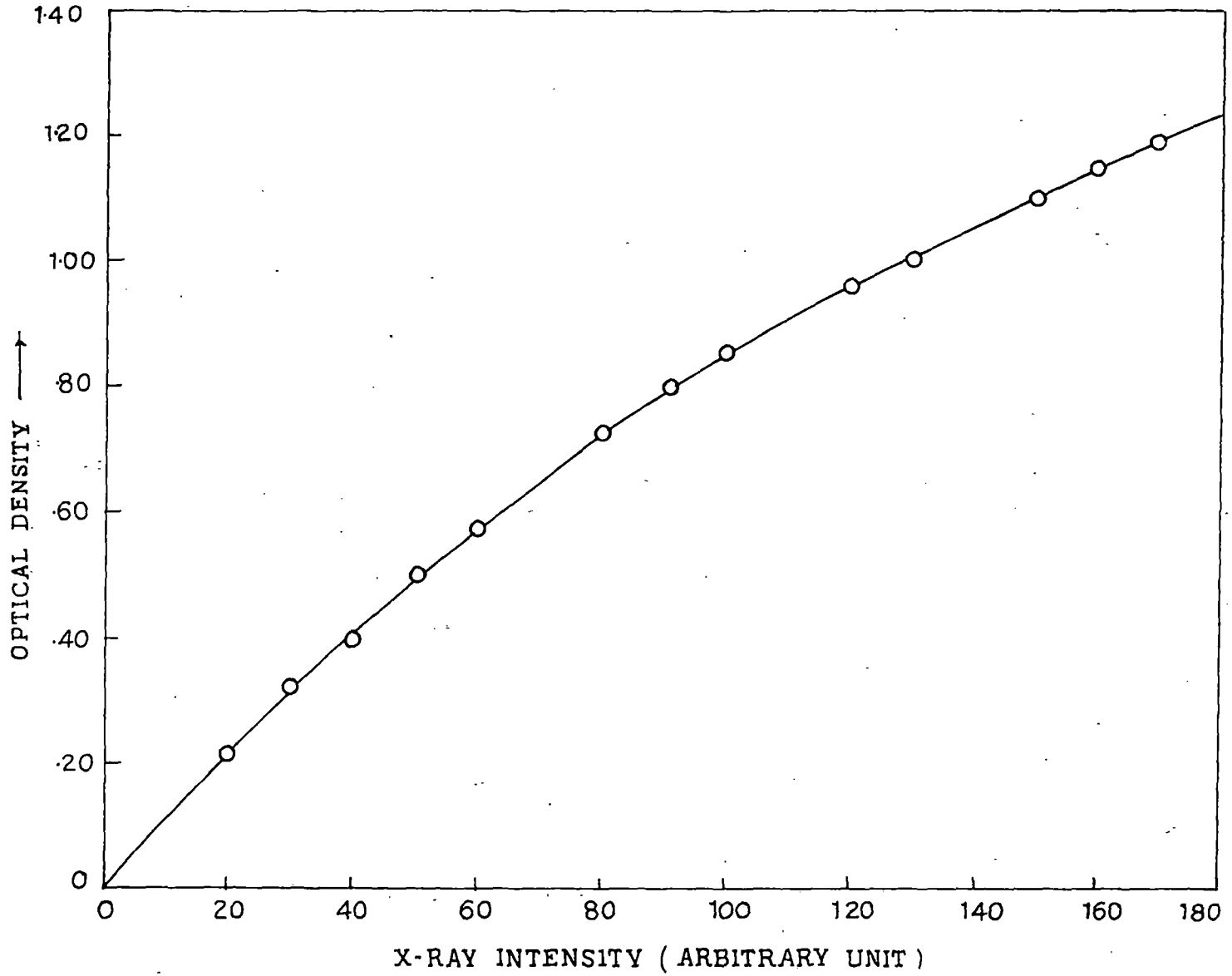

Figure 2.3 Optical density vs. x-ray intensity curve used for calibration.

(b). Circular scaning of x-ray photographs:

A rotating stage was fabricated by us to facilitate full 360° scanning of the photographs. Photographs were scanned to measure angular intensity distribution $I(\theta)$ which was used to calculate the orientational distribution function $f(\beta)$ and order parameters $\langle P_2 \rangle$ and $\langle P_4 \rangle$. The circular scans of the outer diffraction arc was taken from $\psi = 0$ to $\psi = 360^{\circ}$ at about 1° intervals near the peak and at larger intervals elsewhere. The optical density values obtained from the densitometric circular scan were converted to x-ray intensity with the help of calibration curve. Intensity values were then corrected for background intensity values arising due to the air scattering. The peak intensity position which corresponds to $\psi = 0$ was determined from angle vs. intensity curve (Figure 2.4). Taking nineteen $I(\psi)$ values from $\psi = 0$ to $\psi = 90^{\circ}$ at 5° intervals from the smoothed $I(\psi)$ vs. ψ curve, $f(\beta)$, $\langle P_2 \rangle$ and $\langle P_4 \rangle$ were calculated by using Leadbetter's expression mentioned in later part of this chapter. A computer program has been developed for these calculations.

(c). Linear scaning of x-ray photographs:

The diameter of the diffraction rings can be measured from the linear scan of the photographs using the potentiometric recorder and relating optical density vs. linear distance can be plotted.

2.3.2 Orientational distribution functions and order parameters:

Liquid crystals are characterized by an orientational order of their constituent rod like molecules. The examination of the optical properties of nematic and smectic phases show that they have uniaxial symmetry and the axis of uniaxial (cylindrical) symmetry is parallel to a unit vector $\hat{n}$ called the director. A full description of the orientation of such molecules presupposes a knowledge of the distribution functions . The x-ray pattern of oriented samples consist of equatorial arcs. The distribution of intensity along the diffuse equatorial arcs of x-ray pattern

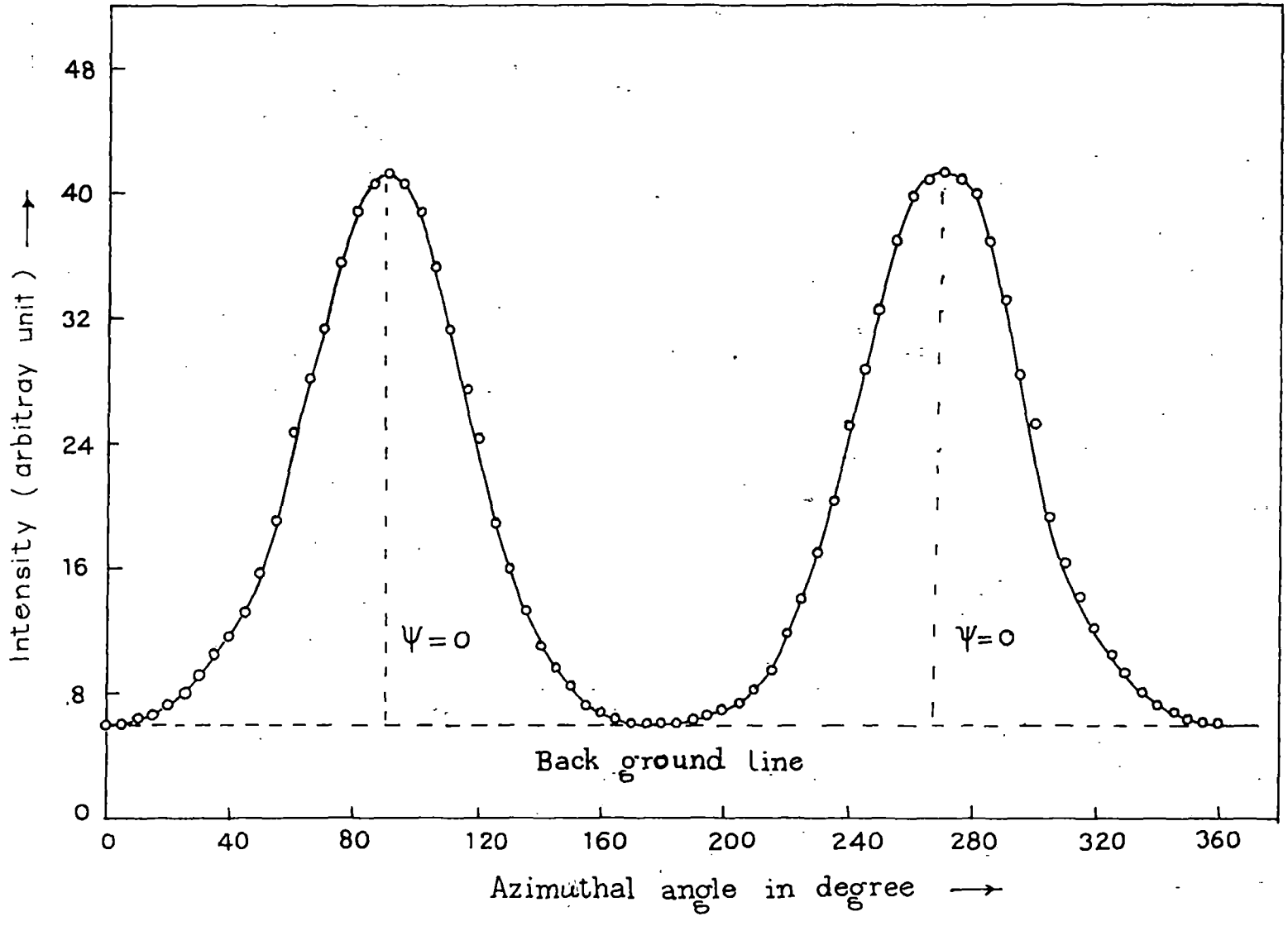

Figure 2.4 Average intensity I(ψ) vs. azimuthal angle (ψ) curve.

(figure 2.1a) is related to the distribution function [24].

$$I(\psi) = c \int_{\beta=\psi}^{\pi/2} [\, f_d(\beta)\, \sec^2\psi\, [\, \tan^2\beta - \tan^2\psi\,]^{-1/2} \sin\beta\, d\beta \qquad 2.15$$

where $f_d(\beta)$ is the distribution function for the orientation β for a local cluster of molecules relative to the director $\bar{n}$ (β = 0). The equation (2.15) can be numerically inverted to give $f_d(\beta)$ and are assumed to be close to the singlet distribution function [24].

The orientational order parameters $\langle P_2 \rangle$ and $\langle P_4 \rangle$ were calculated using the relationship

$$\langle P_L \rangle = \int_0^1 P_L(\cos\beta)\, f_d(\beta)\, d\cos(\beta) \;/\; \int_0^1 f_d(\beta)\, d\cos(\beta) \qquad 2.16$$

with L = 2, 4

In section 2.3.1a the process of measuring the intensity values $I(\psi)$ from the measured optical densities are discussed. I have calculated the intensity values by angular scanning of the x-ray diffraction photograph for ψ = 0 to $\psi = 2\pi$. To calculate $f_d(\beta)$ and order parameter only one quadrant is sufficient. I have calculated all the four quadrant seperately and then taken average values of $I(\psi)$ of the four quadrants, to calculate $\langle P_2 \rangle$ and $\langle P_4 \rangle$ and $f(\beta)$ and obtained almost the same values. Hence, I have used mean $I(\psi)$ values for all calculations. Errors in order parameter values in this manner are estimated to be ± 0.02 for both $\langle P_2 \rangle$ and $\langle P_4 \rangle$.

2.3.3. Molecular parameters for x-ray studies:

The average lateral distance between the neighbouring molecules (D) was calculated from the x-ray diffraction photographs by a formula given by [25]

$$2D \sin\theta = k\lambda \qquad 2.17$$

where 2θ is the Bragg angle for the equatorial diffraction, λ

is the wave length of the x- ray and k is a constant which comes from the cylindrical symmetry of the system. Recent calculations [26] have shown that the value of k depends on the order parameter of the sample under consideration. For perfectly ordered state k = 1.117 as given by de Vries [27]. However, since the variation of k with $\langle P_2 \rangle$ is small, we have used the value k = 1.117 for all our calculations.

For apparent molecular length or layer thickness, d, the Bragg equation was used ($2d \sin \theta = \lambda$), where θ is the Bragg angle for the meridional diffraction crescent for an aligned sample or for the inner halo in the case of unaligned samples.

2.3 Refractive index of mesophases:

In liquid crystalline phases refractive indices are important parameters for technical application. The first birefringence measurements were made by E. Dorn [28]. The theoretical explanation of the birefringence have been made by O. Weiner [29]. and H. Zocher [30,31]. In liquid crystals due to the anisotropic molecular arrangements, it was necessary to take into account the effect of the anisotropic internal field in evaluating the polarizabilities. Hence, in case of liquid crystals the well known Lorenz- Lorentz formula for isotropic media should be replaced by Neugebauer's [32]. relations or Vuk's formula [33]. Saupe and Maier [34] also applied a more elaborate form of internal field suggested by Neugebauer.

In this study, I have measured the ordinary and extraordinary refractive indices n_o and n_e for different liquid crystal samples and have calculated the effective polarizabilities α_o and α_e of anisotropic liquid crystals by using the two different internalfield models [32,33]. Finally orientational order parameter $\langle P_2 \rangle$ was calculated.

(a) Neugebauer's method :

Neugebauer [32] extended Lorenz-Lorentz equations for an isotropic system to an anisotropic system. The effective

polarizabilities α_e and α_o of the liquid crystals are given by,

$$n_e^2 - 1 = 4\pi N\alpha_e \ (1 - N\alpha_e\gamma_e)^{-1} \qquad 2.18$$

$$n_o^2 - 1 = 4\pi N\alpha_o \ (1 - N\alpha_o\gamma_o)^{-1} \qquad 2.19$$

where N is the number of molecules per c.c and γ_i's are internal field constants, n_e and n_o, the extraordinary and ordinary refractive indices respectively. The equations for calculating the α_o and α_e obtained from equations (2.18) and (2.19) are

$$\frac{1}{\alpha_e} + \frac{2}{\alpha_o} = \frac{4\pi N}{3}\left[\frac{n_e^2 + 2}{n_e^2 - 2}\right] + \left[\frac{2(n_o^2 + 2)}{n_o^2 - 1}\right] \qquad 2.20$$

and

$$\alpha_e + 2\alpha_o = \frac{9}{4\pi N}\left[\frac{n^2 - 1}{n^2 + 2}\right], \qquad 2.21$$

where $n^2 = 1/3\ (n_e^2 + 2n_o^2)$

Solving equations 2.20 and 2.21 α_o and α_e values can be obtained..

(b) Vuks Method:

Vuks has derived another formula for polarizabilities associated with anisotropic organic molecules. The principal polarizabilities and refractive indices can be expressed as

$$\frac{n_e^2 - 1}{\bar{n}^2 + 2} = \frac{4\pi N}{3}\alpha_e \qquad 2.22$$

$$\frac{n_o^2 - 1}{\bar{n}^2 + 2} = \frac{4\pi N}{3}\alpha_o \qquad 2.23$$

where $\bar{n}^2 = \frac{1}{3}\ (n_e^2 + 2n_o^2)$ and α_e and α_o can be calculated directly from the refractive index values.

2.4.1. Calculation of order parameters from polarizabilities:

The principal polarizabilities (α_o,α_e) have been calculated by using Vuks' isotropic model and Neugebauer's relations (anisotropic model). It can be shown that

$$\alpha_e = \bar{\alpha} + \frac{2}{3}\alpha_a \langle P_2 \rangle \qquad 2.24$$

$$\alpha_o = \bar{\alpha} - \frac{1}{3}\alpha_a \langle P_2 \rangle \qquad 2.25$$

where $\bar{\alpha} = (2\alpha_o + \alpha_e)/3$ is the mean polarizability. $\alpha_a = (\alpha_\parallel - \alpha_\perp)$ is the molecular polarizability anisotropy where $\alpha_\parallel$ and $\alpha_\perp$ are the principal polarizabilities, parallel and perpendicular to the long axes of the molecules in the crystalline state, which are not however available.

To get the values of $(\alpha_\parallel - \alpha_\perp)$ the widely used method of Haller et al [35] was adopted. A graph was plotted with $\log(\alpha_e - \alpha_o)$ versus $\log(T_c - T)$, where T_c corresponded to the nematic isotropic transition temperature. The plot which is found to be a straight line is extrapolated to T = 0, giving $(\alpha_e - \alpha_o)_{T=0} = (\alpha_\parallel - \alpha_\perp)$. For each case a set of values of α_e, α_o and $(\alpha_\parallel - \alpha_\perp)$ were obtained (Figure 2.5) and then from the relation

$$\langle P_2 \rangle = \frac{\alpha_e - \alpha_o}{\alpha_\parallel - \alpha_\perp} \qquad 2.26$$

order parameters $\langle P_2 \rangle$ was calculated.

2.4.2 Measurement of refractive indices:

The refractive indices n_e and n_o for extraordinary and ordinary ray were measured by a thin prism technique. The refracting angle of the prism was less than 2^o. The details of the preparation of the prism and the experimental procedure have already been

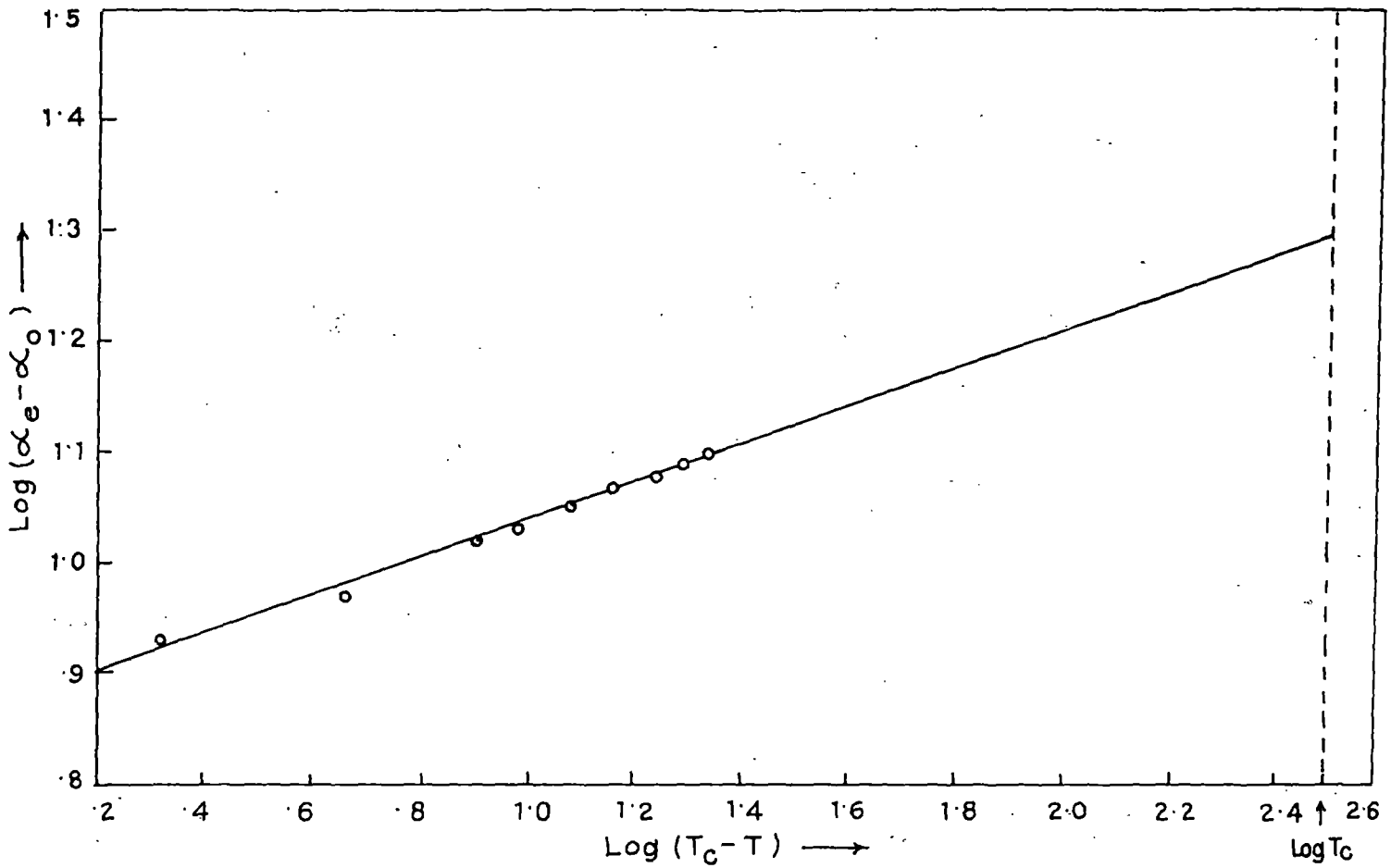

Figure 2.5 Typical log ($\alpha_e - \alpha_o$) vs. log ($T_c - T$) curve (mixture F (x= 0.7316), Chapter 4).

reported by Zemindar et al [36]. For the preparation of a prism two clean optically plane glass plates were used. One surface eachof the glass plates was rubbed parallel to direction of one of their edges. The plates were then treated with a dilute solution of polyvinyl alcohol and then dried. The prefered direction on the substrate can be obtained by rubbing the same surface in the same direction again by a tissue paper. The prism was then formed by placing the treated surfaces inside and the rubbing direction parallel to the refracting edge of the prism. A thin spacer was placed at the thick edge of the prism for getting the desired refracting angle of the prism. The sides of the prism were sealed with a high temperature adhesive. Liquid crystal sample was placed inside through open top side of the prism and heated to the isotropic state and then cooled down very slowly and the process was repeated several times. No magnetic field was applied. Repeated heating and cooling produced a homogeneous nematic sample with optic axis parallel to the refracting edge of the prism. Only those prisms, which showed uniform alignment of the liquid crystals under polarizing microscope, were used. The prism was then placed in a brass chamber, with transparentwindows, whose temperature could be maintained by a temperature controller (Indotherm model 401) at any desired value to an accuracy of $\pm$ $0.5^{o}C$ by means of an electric oven. The refractive indices were measured for three wavelengths (λ = 6907$\mathring{A}$, 5890$\mathring{A}$, 5461$\mathring{A}$) from a mercury lamp by means of a precision spectrometer, a wavelength selector and a Nicol prism.

2.5 Measurement of Densities :

The densities of the liquid crystals were measured with the help of a dilatometer of the capillary type. A weighed sample of the liquid crystal was introduced inside the capillary tube of the dilatometer and it was placed in a thermostated water bath. Sufficient time was allowed for equilibrium at any desired temperature before taking each readings. The length of the liquid crystal column was measured at differnt temperatures with a travelling microscope. The densities were calculated after

correction of the expansion of the glass. The accuracy of the measurement of the densities was within 0.1%.

2.6 Elastic Constant and deformation free energy of nematic liquid crystal:

Many of the important physical properties involving the response of the bulk liquid crystal samples can be described by regarding the liquid crystal as a continuous medium. Based on this point of view , Zocher [37], Osceen [38] and Frank [39] developed a phenomenological continuum theory which can explain various field induced effect of liquid crystals.

According to this theory, the elastic deformation free energy density can be written as:

$$F_{def} = (1/2)\ [K_1 (div\hat{n})^2 + K_2(\hat{n}.curl\hat{n})^2 + K_3(\hat{n}\times curl\hat{n})^2] \qquad 2.27$$

where K_1, K_2, K_3 refers to the splay, twist and bend elastic constants respectively and $\hat{n}$ is the director.

2.6.1 Freedericksz transition:

Various methods have been used to measure the elastic constants of nematic liquid crystals. One of the most simple and convenient methods is Freedericksz transition, where an electric [40-43] or magnetic [44-51] field is applied to deform a thin layer of surface aligned nematogenic sample. Below a critical field the sample remains surface aligned, but above it starts to align itself along the external field for nematogens having positive anisotropy ($\Delta\varkappa > 0$ or $\Delta\varepsilon > 0$). This phenomenon is known as Freedericksz's transition. Depending on the geometry of the arrangement, splay, twist or bend elastic constant can be determined from Freedericksz transition in a magnetic field as shown in figure 2.6.

To have a clear idea I shall discuss the situation of a uniform planar layer of thickness d (Fig. 2.7a-2.7e) i.e splay mode only.

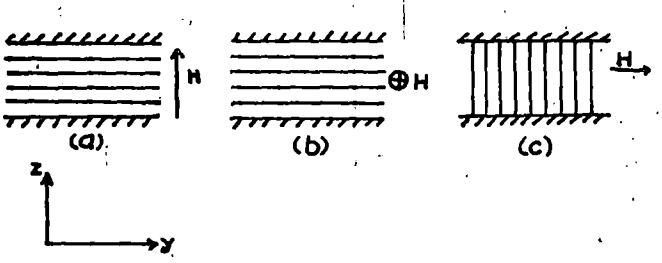

Figure 2.6. Schematic experimental set-up for the determination of elastic constants from Freedericksz transition: (a) splay, (b) twist, (c) bend.

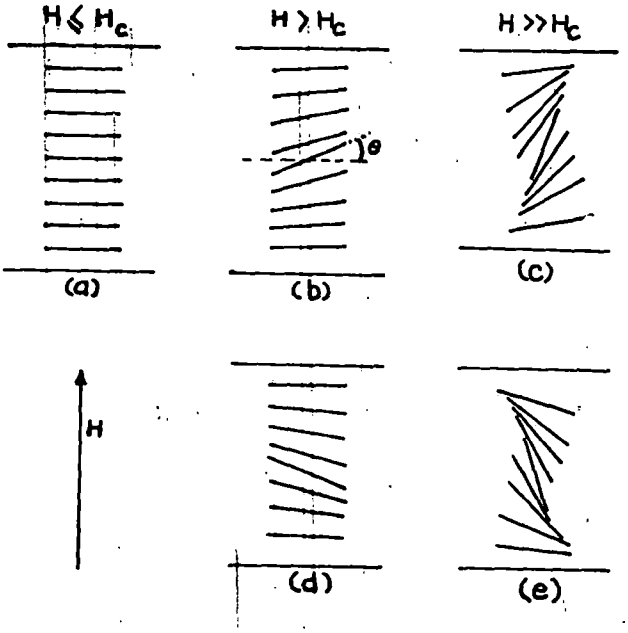

Figure 2.7. Deformation of the director pattern above the threshold in the case of splay mode.

A magnetic field is applied in the Z direction as shown in figure 2.6(a). When the field is gradually increased, there is a gradual change in the director pattern once H exceeds a critical value H_c. When $H < H_c$, the director is everywhere in the y direction, Although there is a small fluctuation of the director as the stabilizing elastic torque is greater than the destabilizing magnetic torque an equlibrium planar texture is maintained. For H slightly greater than H_c the system is in unstable equlibrium state. At slightest perturbation the system jumps to one of the two stable states, (b) or (d) as shown in figure 2.7.

The threshold magnetic field for all the three geometries can be obtained in a generalised form as

$$(H_c)_i = (K_i/\Delta\varkappa)^{1/2} \frac{\pi}{d} \qquad 2.28$$

i = 1,2,3 refer to the splay, twist and bend deformations respectively, d is the thickness of the liquid crystal layer, $\Delta\varkappa$ is the diamagnetic anisotropy. and $(H_c)_i$ is the respective critical magnetic field.

2.5.2 Description of experimental setup for determination of K_1 and K_3.

A block diagram of the experimental setup for studying elastic constants by Freedericksz transition method is shown in figure 2.8 The monochromatic light beam (sodium D light) is incident on the sample, which is mounted in a brass oven (o), after passing through a lens (L), polarizer (P) and collimating pinholes (C_1, C_2). The temperatures are mesaured and regulated with an accuracy $\pm$ 0.2°K with the help of a thermocouple inserted in the block containing the sample and a temperature regulator (Indotherm model 457). The transmitted light intensity is detected by a photomultipier tube (M) for photon counting. An analyser is placed in front of the P.M. tube. The polariser and analyser are placed in crossed position. The magnetic field H is applied perpendicular to the direction of the preferred orientation of the liquid

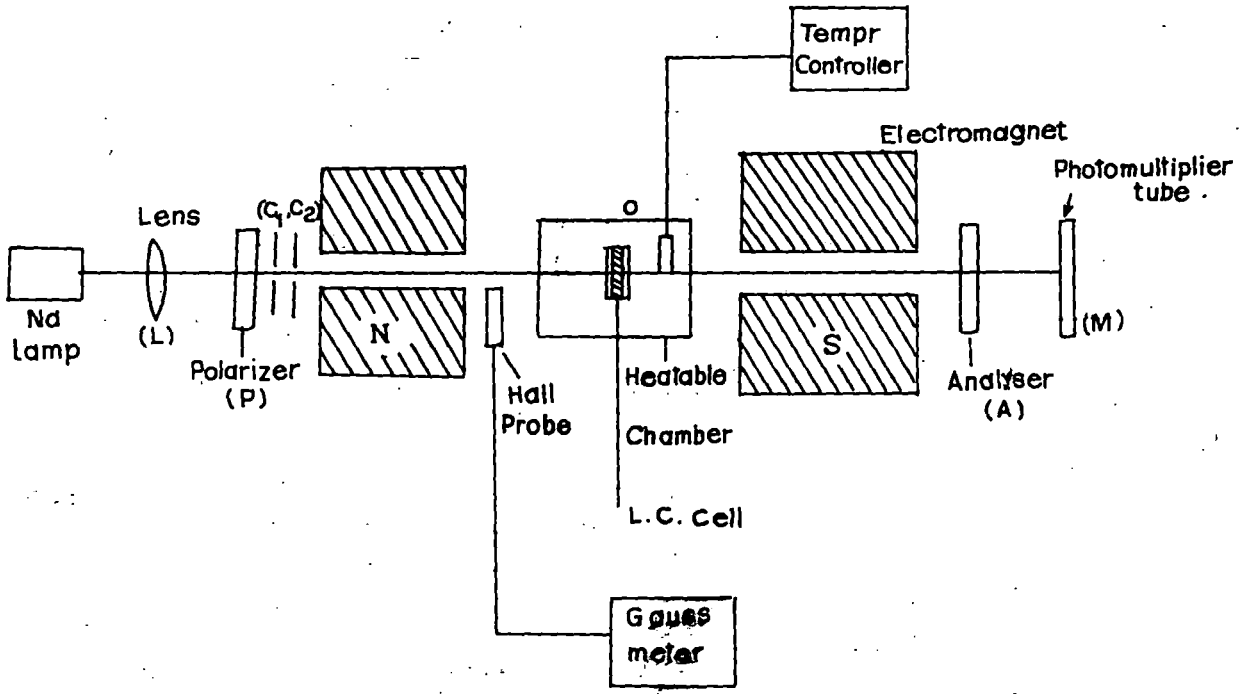

Figure 2.8. Block diagram of the experimental set-up for measuring elastic constants by Freedericksz transition.

crystal sample. The field is changed slowly so that the nematic orientation remain in equlibrium with the applied magnetic field. The intensity of the transmitted light is measured as a function of the applied magnetic field for any desired temperature. It is observed that when the field H reaches a critical value H_c the optical properties of the sample change drastically and thus value H_c can be measured from field versus intensity curve within an accuracy of ± 10 gauss. The magnetic field is measured by a sensitive Gaussmeter(Model DGM-102). For the determination of actual threshold it is necessary to maintain the direction of the director exactly normal to the applied magnetic field.

The sample is taken between two plane parallel glass plate separated by a glass spacer of thickness 160μm or 320μm. The glass plates are cleaned by different cleaning agent and subsequently dried and treated for homeotropic or homogeneous alignment as required (details of the technique has been given in detail by de Jeu [52]). The splay elastic constant (K_1) is measured using cells with homogeneous planar alignment where inside surface of the glass plates are treated with 1.0% aquous solution of polyvinyl alcohol, dried and then rubbed unidirectionally with tissue paper. In case of bend elastic (K_3) constant measurement it is necessary to treat the glass plates with dilute solution of cetyl trimethyl ammonium bromide in acetone to get homeotropic alignment and using the geometrical arrangement shown in figure 2.6(c).

The thickness of the cells are measured by a microscope . I had to work with rather thick samples, because of the limitation of the available magnetic field.

Actually, the experiment for the determination of K_1 and K_3 consists of measuring the variation of birefringence of light incident normal to the liquid crystal film. A linealy polarized light incident on the film and the suitable analyser C (i.e., a combination of $\lambda/4$ plate and a linear polariser) is used to detect the transmitted light intensity. When the fields exceeds a critical value H_c the transmitted intensity shows a sudden change. If the field is gradually increased further, the intensity exhibits oscillations becauses of the change of the phase retardation.

The threshold field for twist deformation cannot be detected optically when viewed along the twist axis. The large birefringence of the medium for this direction of propagation, the state of polarization of the transmitted beam is indistinguishable from that of the emerging beam from the untwist nematic. A total internal reflection technique can be used to measure the K_2 values of the twist deformation. However, I have measured only K_1 and K_3 for four different nematic liquid crystals.

2.5.3 Molecular theory of elastic constants:

There are several theories of elastic constants of nematogens, but probably the simplest one is due to Priest [53]. He has expressed the elastic constants as a function of $\langle P_2 \rangle$ and $\langle P_4 \rangle$ of the length to width ratio of the molecules, assumed to be spherocylinders. The following equations are found

$$K_1 = \bar{K}(1 + \Delta - 3\Delta'\gamma) \qquad 2.29a$$

$$K_2 = \bar{K}(1 - 2\Delta - \Delta'\gamma) \qquad 2.29b$$

$$K_3 = \bar{K}(1 + \Delta + 4\Delta'\gamma) \qquad 2.29c$$

where

$$\bar{K} = (K_1 + K_2 + K_3)/3 \qquad 2.30a$$

$$\gamma = \langle P_4 \rangle / \langle P_2 \rangle \qquad 2.30b$$

The quantities Δ and Δ' are constants depending on molecular properties. Considering molecules to be spherocylinders, interacting via hard core repulsion, one finds [53,54],

$$\Delta = (2R^2 - 2) / (7R^2 + 20) \qquad 2.30c$$

$$\Delta' = (9/16) (3R^2 - 8) / (7R^2 + 20) \qquad 2.30d$$

$$R = (L - D) / D, \qquad 2.30e$$

L and D are the overall length and the width of the spherocylinder respectively.

It is clear from the above equations that for any reasonable length to width ratio Δ and Δ' should be positive. Hence, $K_2 < K_1$

$<K_3$, for positive Δ' and γ. It is seen that for positive values of γ, the values of K_3/K_1 tends to increase with increasing length/width ratio, in good agreement with the experimental results for rigid molecules [55].

Structure and chemical name of the liquid crystals studied.

The liquid crystals studied in the present investigations were obtained from well known chemical firms like E.Merck, U.K., Hoffmann-La Roche, Basel, Switzerland. These samples were used fresh from the package without further purification.
A list of the names of the liquid crystals and their structural formulae is given below.

1. 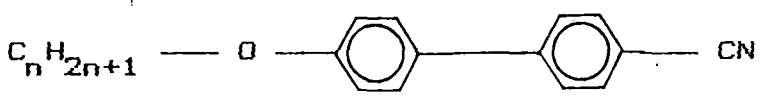

(i) n = 6, 1 cyano- biphenyl-hexyl- ether (6OCB in short).
(ii) n = 8, 1 cyano- biphenyl-octyl- ether (8OCB in short).
(iii) n = 9, 1 cyano- biphenyl-nonyl- ether (9OCB in short).
(iv) n = 10, 1 cyano- biphenyl-decyl- ether (1OOCB in short).
(v) n = 11,1 cyano- biphenyl-undecyl- ether (11OCB in short).
(vi) n = 12, 1 cyano-biphenyl-dodecyl- ether (12OCB in short).

2. 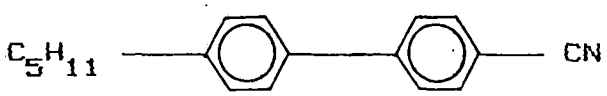

4-n-pentyl-4-n'-cyanobiphenyl (5CB in short).

3. 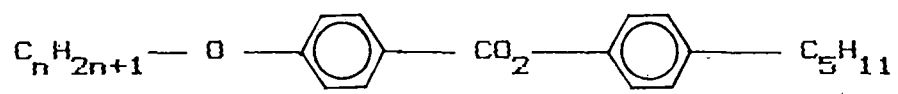

(i) n = 5, 4-n-pentyl phenyl-4-n' pentyloxy benzoate (ME 5O.5 in short).

(ii) n= 6, 4-n-pentyl phenyl-4-n' hexyloxy benzoate (ME 6O.5 in short).

4. 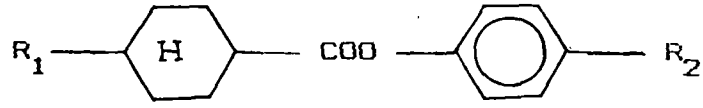

(i) R_1= C_5H_{11}, R_2= OCH_3, p- methoxyphenyl trans-4-pentyl cyclohexane carboxylate (MPPCC in short).

(ii) R_1= C_5H_{11}, R_2= OC_3H_7, p- propoxyphenyl trans-4-pentyl cyclohexane carboxylate(PPPCC in short).

(iii) R_1= C_4H_9, R_2= OC_2H_5, p- ethoxyphenyl trans-4-butyl-cyclohexane carboxylate (EPBCC in short).

(iv) R_1= C_5H_{11}, R_2= CN, p- Cyanophenyl trans-4-pentyl cyclohexane carboxylate (CPPCC in short).

References

[1]. E.B. Priestley, P.J.Wojtowicz and P. Sheng, eds., Introduction to Liquid Crystals, Plenum, New York, (1974).

[2]. S. Chandrasekhar, Liquid Crystals, Cambridge University Press, Cambridge,(1977).

[3]. G. Vertogen and W.H. de Jeu, Thermotropic Liquid Crystals, Fundamentals, Springer-Verlag (1988).

[4]. G.R. Luckhurst and G.W. Gray, (Editors) The Molecular Physics of Liquid Crysals, Academic Press (1979).

[5]. P. G. de Gennes, The Physics of Liquid Crystal, Clarendon Press, Oxford,(1974).

[6]. A. Saupe and W. Maier Z. Natureforsch, **14a**, 882 (1959) and **15a**, 287 (1960).

[7]. W.L. McMillan, Phys. Rev., **A4**, 1238 (1971).

[8]. W.L. McMillan, Phys. Rev., **A6**, 936 (1972).

[9]. E.B. Priestley, P.S. Pershan, R.B. Meyer and D.H. Dolphin, Vijnana Parishad Anusandhan Patrika **14**, 93 (1971).

[10]. K.K. Kobayashi, J. Phys., Soc. (Japan), 29, 101 (1970).

[11]. K.K. Kobayashi, Mol. Cryst. Liq. Cryst., **13**, 137 (1971).

[12]. D. Demus and L. Richter, Textures of Liquid Crystals, Verlag Chemie, New York (1978).

[13]. Advances in Liquid Crystals, Vol 6, Ed. G.H. Brown Academic Press (1983), Chapter 1.

[14]. B.K. Vainstein, Diffraction of X- rays by Chain Molecules, Elsevier, Pub. Co. (1966).

[15]. I. G. Chistyakov, Sov. Phys. Vsp. 9, 551 (1967).

[16]. L.A. Azaroff, Mol. Cryst. Liq. Cryst., 60, 73 (1980).

[17]. J. Falguerettes and P. Delord, Liquid Crystals and Plastic Crystals, Eds. G.W. Gray and P. A. Winsor, Ellis Horwood, vol. 2, Ch.3 (1974).

[18]. H. Kekler and R. Hartz, Hand book of Liquid crystals, Verlag Chemie, Ch. 5 (1980).

[19]. A.J. Leadbetter, The Molecular Physics of Liquid Crystals, Eds. G. R. Luckhurst & G.W. Gray, Chapter 13, Academic Press (1979).

[20]. P.S. Pershan, Structure of Liquid Crystal Phases, World Scientific (1988).

[21]. B. Jha and R. Paul, Proc. Nucl. Phys. Solid State Phys. Symp., India, 19c, 491 (1970).

[22]. C. Kittle, Int. to Solid State Phys, Wiley Eastman, Ch 2 (1976).

[23]. H.P. Klug and L.E. Alexander, X-ray diffraction procedures, John Wiley and Sons, N Y, Page 114 and 473 (1974).

[24]. A.J. Leadbetter and E.K. Norris, Mol. Phys.,38, 689 (1979).

[25]. J.H. Wendroff and E.P. Price, Mol. Cryst. Liq. Cryst., 24, 129, (1973).

[26]. R. Paul. and G. Chaudhuri, Abstract in the 14th International Liquid Crystal Conference, Pisa, 1992, Abs-no-H- P23.

[27]. A. de Vries, Mol. Cryst. Liq. Cryst., 10, 31 and 219 (1970).

[28]. E. Dorn, Z. Physik, 11, 111 (1910).

[29]. O. Weiner, S. Ber. Sächs. Ges. Wissensch., 61, 113 (1909).

[30]. H. Zocher, Naturwiss., 13, 1015 (1925).

[31]. H. Zocher, Z. Krist.,79, 122 (1931).

[32]. H. E. Neugebauer, Canad. J. Phys., 32, 1 (1954).

[33]. M. F. Vuks, Optics and Spectroscopy, 20, 361 (1966).

[34]. A. Saupe and W. Maier Z. Natureforsch, 16a, 816 (1961).

[35]. I. Haller, H.A. Huggins, H.R. Lilienthal and T.R. McGuire, J. Phys. Chem.,77, 950 (1973).

[36]. A.K. Zeminder, S. Paul and R. Paul, Mol. Cryst. Liq. Cryst., 61, 191 (1980).

[37]. H. Zocher, Trans Faraday Soc., 29, 945 (1933).

[38]. C.W. Oseen, Trans Faraday Soc., 29, 883 (1933).

[39]. F.C. Frank, Faraday, Soc. Discussion 25, 19 (1958).

[40]. H. Gruler, T.J. Schiffer and G. Meier, Z. Natureforsh, 27a, 966 (1972).

[41]. H. Gruler and L. Cheung, J. Appl. Phys. 46, 5097 (1975).

[42]. H. Deuling in Liquid Crystals, Solid State Physics Suppl. no. 14, ed. L. Liebert p.77, Academic Press (New York).

[43]. M.J. Bradshaw and E.P. Raynes, Mol. Cryst. Liq. Cryst., 72, 35 (1980).

[44]. V. Freedericksz and V. Tsvetkov, Phy. Z. Soviet Union, 6, 490 (1934).

[45]. V. Freedericksz and V. Zolina, Trans. Faraday Soc. 29, 919 (1933).

[46]. P.P. Karat and N.V. Madhusudana, Mol. Cryst. Liq. Cryst., 40, 239 (1977).

[47]. H.P. Schad and M.A. Osman, J. Chem. Phys. 75 (2) 880 (1981).

[48]. F. Leenhouts, H.J. Boeber, A.J. Dekker and J.J. Jonker, J. Phys. (Paris) Colloque 40, C3-291 (1979).

[49]. H.P. Schad, G. Bauer and G. Maier, J. Chem. Phys. 67, 3705 (1977).

[50]. F. Leenhouts and A. J. Dekker, J. Chem Phys, 74, 1956 (1981).

[51]. H.P. Schad and M.A. Osman, J. Chem. Phys. 75 (2) 880 (1978).

[52]. W. H. de Jeu, Physical properties of Liquid Crystalline materials, Gordon and Breach, Chapter 2, (1980),

[53]. R. G. Priest, Phys. Rev. A7, 720 (1973), Mol. Cryst. Liq. Cryst. 17, 129 (1972).

[54]. J.P. Straley. Phy. Rev. A8, 2181 (1973).

[55]. F. Leenhouts, A.J. Dekkar amd W.H. de Jeu, Phys. Lett. 72A, 155 (1979).